PCCP

Accepted Manuscript

ROYAL SOCIETY OF CHEMISTRY

www.rsc.org/pccp

Physical Chemistry Chemical Physics
CREATED USING THE RSC LaTeX PCCP ARTICLE TEMPLATE – SEE www.rsc.org/electronicfiles FOR DETAILS
ARTICLE TYPE www. rsc.org/xxxxxx | XXXXXXXX

Structure, fragmentation patterns, and magnetic properties of small cobalt oxide clusters

R. H. Aguilera-del-Toro,[a] F. Aguilera-Granja,[a,b] A. Vega,[c] and L. C. Balbás,[c]

Received Xth XXXXXXXXXX 20XX, Accepted Xth XXXXXXXXX 20XX
First published on the web Xth XXXXXXXXXX 200X
DOI: 10.1039/b000000x

The favorable stoichiometry of $Co_nO_m^+$ clusters has been recently determined by means of multiphoton dissociation of oxide clusters beams coming from laser evaporation of metal rods seeded with 0.5-5% oxygen and selected by time of flight mass spectroscopy. It was observed that the prominent stoichiometry is $n = m$, and that the preferred dissociation channel is the loss of O_2 molecules. The $Co_4O_4^+$ cluster results to be particularly abundant, an indication of its high stability. In this work we present density functional calculations, within the generalized gradient approximation, for the geometric, electronic, and magnetic properties of neutral and cationic $Co_nO_m^{0/+}$ clusters with n = 3-8 and m = 1-10. The ionic structures were determined after optimizing several initial geometries selected from previous pure Co clusters calculations, with consecutive adsorbed oxygen atoms, as well as geometries constructed by assembling several CoO units and adding subsequent oxygen atoms. The fragmentation patterns were studied by comparing the energy separation of O_2, CoO, Co_2O, CoO_2, and Co, fragments. We obtain that the preferred fragmentation channel is the loss of O_2, that the favourable stoichiometry is 1:1, and that $Co_4O_4^+$ is especially stable, in full agreement with the experiments. In addition are studied in detail the magnetic properties related to spin isomeric configurations of $(CoO)_n^+$ clusters.

1 Introduction

Transition metal oxides are the basic components of many applications, such as heterogeneous catalysis, electronics, magnetism, among others in material science.[1] From the second part of the last century to present time, the properties of magnetic nanoparticles of transition metal oxides is a subject of great interest, both scientific and technological. However, the techniques of fabrication of nanoparticles with prefixed structural and chemical properties are available only along the last twenty years. Due to the large ratio of surface to volume of small atomic clusters, their properties are different from those of the bulk matter.[2] This fact confers to each specific cluster an unique entity.

The transition metal oxides show a great variety of crystallographic and magnetic structures. The magnetic exchange interaction is favored by the oxygen ions, and the resulting effective interaction is strongly dependent on the metal coordination number. Thus, from the point of view of the structural and magnetic properties, the oxygen-metal bond, which is stronger than the metal-metal bond, makes the formation process of small nanoparticles even more interesting than that of the bulk oxide. That is, the equilibrium structure of a metal oxide cluster is a delicate balance between bulk-like bonds and surface-like bonds.

Small clusters with a few hundred atoms can be produced by laser vaporization techniques. However, a low density of particles is achieved, which precludes their characterization by means of the usual spectroscopic and crystallographic techniques (see for example Mordy and coworkers[3]). Nevertheless, the vibrational properties of small metal-oxide clusters from laser vaporization sources can be studied by means of multiple absorption of infrared photons.[4–6] These experiments, combined with density functional theory (DFT) calculations, allows the determination of the geometrical structure of the low lying energy isomers of clusters with less than 20 atoms (see, for example the recent work of Harding and Fielicke[7]). Other experimental techniques appropriated for the structural determination of the cluster geometry, when combined with accurate DFT calculations, are the photoelectron spectroscopy (PES)[8,9] and the Ion Mobility Mass Spectrometry (IMMS).[10,11] In the work of Ota and coworkers[10] it is concluded that $(CoO)_{3-5}^+$ must exhibit ring-like structure (with CoO units), whereas $(CoO)_{6,7}^+$ show a compact tower-like structure. From a pure *ab-initio* calculation was determined recently[12] that neutral Co_2O_2 shows planar ring structure only for the high spin configuration with multiplicity equal seven. In a similar approach to that in the work of Ota *et al.*[10], it was concluded that two- and three-dimensional structural isomers coexist for $(FeO)_{6-8}^+$ clusters.

[a] *Instituto de Física, Universidad Autónoma de San Luis Potosí, San Luis Potosí, México*
[b] *DIPC Donostia International Physics Center, E-20018 San Sebastian, Spain*
[c] *Departamento de Física Teórica, Atómica y Óptica, Universidad de Valladolid, E-47011 Valladolid, Spain.*

An example of the vibrational spectroscopy combined with DFT calculations approach was the determination of a ferromagnetic ground state for small $(CoO)_n$ clusters[4], in contrast with the well known antiferromagnetic state of bulk CoO material. In other cases, pure calculations are used to establish fundamental properties of the metal oxide bonds. For example, in a recent *ab initio* simulation of the laser ultrafast spin dynamics on homonuclear iron- and nickel-oxide clusters[13] was established that the oxygen prefers bridge sites between metal atoms which leads to a well defined spin localization. Thus, spin-flip and spin-transfer scenarios appear in FeOFe and FeOOFe clusters, but only spin-flip occurs on NiONi and NiOONi. These facts have potential applications in spintronics.

The role of cluster ion structure in reactivity and collision-induced dissociation of $Co(CoO)_x^+$, $(CoO)_x^+$, and $(CoO)_xO^+$ cationic clusters was studied by combining mass spectrometric experiments and calculations (within a pair potential model) in an earlier paper.[14] More recently, it was studied the formation and distribution of iron- and cobalt-oxide cationic clusters by means of mass spectroscopy of supersonic jets of clusters produced by laser ablation.[15] It was observed that the distribution of $Co_nO_m^+$ grown in an oxygen saturated atmosphere is more complex than that for $Fe_nO_m^+$ clusters. Thus, the observed favorable stoichiometries of $Co_nO_m^+$ appear for (n,m) = (11,12) and (12,12), whereas the cases (11,13) and (12,13) were not observed. DFT calculations in that work for the cases (n,n) with n = 2, 3, 4, 6, 9, and 12, found that cage-like or tower-like type of structures were more stable than the typical NaCl structure of bulk CoO oxide.

The favorable stoichiometries of $Co_nO_m^+$ and $Ni_nO_m^+$ clusters have been recently determined by means of photodissociation of beams coming from laser evaporation and selected by time of flight mass spectroscopy.[16] It was obtained that the prominent stoichiometry of $Co_nO_m^+$ is $n = m$, and that of $Ni_nO_m^+$ is $m = n - 1$ in competition with $n = m$. For $Co_nO_m^+$ the preferred dissociation channel is the loss of O_2 molecules. The $Co_4O_4^+$ cluster results to be particularly abundant, a clear indication of its high stability.

In this work we report first principles DFT calculations within the generalized gradient approximation (GGA), for the geometrical, electronic, and magnetic properties of neutral and cationic $Co_nO_m^{0/+}$ clusters with n = 3-9 and m = 2-9. In section 2 are given details of the calculations, and the results are presented in different subsections of section 3: in subsection 3.1 are discussed the ionic structures and electronic properties like binding energy, HOMO-LUMO gap, and ionization potential; in subsection 3.2 fragmentation channels are studied by comparing the minimum energy needed for the separation of O_2, CoO, Co_2O, CoO_2, and Co, fragments; in subsection 3.3 are studied the magnetic properties related to isomeric configurations of $(CoO)_n$ clusters, in particular the highly magnetic $(CoO)_4$ one. In section 4 are collected the main conclusions.

2 Theoretical approach and computational details

We performed fully self-consistent DFT calculations using the SIESTA code[17], which solves the spin-polarized Kohn-Sham equations within the pseudopotential approach. For the exchange and correlation potential we used the Perdew-Burke-Ernzerhof form of the generalized gradient approximation (GGA).[18] We employed norm-conserving scalar relativistic pseudopotentials[19] in their fully nonlocal form[20], generated from the atomic valence configuration $3d^84s^1$ for Co (with core radii 2.00 a. u. for s, p and d orbitals), and $2s^22p^4$ for O (with core radii 1.14 a.u. for s, p and d orbitals) Nonlinear partial core corrections[21], which are known to be important for transition metal pseudopotential, are included for Co at the core radius 0.7 Å.

Valence states were described using double-ζ basis sets for O and Co, with maximum cutoff radii radius 4.931 Å ($2p$) and 7.998 Å ($3d,4s$), respectively. A $4p$ polarization orbital was also considered for Co, with cutoff radius 7.998 Å. The energy cutoff used to define the real-space grid for numerical calculations involving the electron density was 250 Ry. The Fermi distribution function that enters in the calculation of the density matrix was smoothed with an electronic temperature of 25meV. We used an energy criterium of 10^{-4} eV for converging the electronic part.

In the calculations, the individual clusters were placed in a cubic supercell of $20 \times 20 \times 20$ Å^3, a size large enough to neglect the interaction between the cluster and its replicas in neighboring cells. It was considered only the Γ point ($k = 0$) when integrating over the Brillouin zone, as usual for finite systems.

The equilibrium geometries resulted from an unconstrained conjugate-gradient structural relaxation using the DFT forces. Initial geometries were built by considering different arrangements of the Co and O atoms without privileging those formed from given Co subclusters. Thus, an exhaustive sampling of possible geometries was tested, including those in which the possibly strong Co-O bonding prevents the nucleation of compact Co subclusters. Structures were relaxed without any symmetry constraint until interatomic forces were smaller than 0.003 eV/Å. In all cases different spin isomers were checked in order to ensure the correct ground state. For the search of spin isomers of $Co_nO_n^+$ clusters the criterium for maximum interatomic forces was further reduced to 0.001eV/Å.

For selected clusters, we performed a benchmark against results obtained using the VASP code[22,23] with the PBE functional. VASP employs a plane-waves basis set instead of numerical pseudoatomic orbitals, and the core interactions are

treated be means of the projector-augmented wave (PAW) approach instead of pseudopotentials. In all cases the agreement with our SIESTA setup was fine.

3 Results and discussion

3.1 Geometrical configurations and electronic properties

In the following we comment on the main structural features of the optimized $Co_nO_m^+$ clusters. These clusters are denoted as (n,m) in general, or well as $n.m$-Label (Label= I, II, ...) in correspondence with the notation for the structures depicted in Figures 1, 2, 3, and 4. We will restrict the discussion to the lowest energy isomers (denoted $n.m$-I, in those figures), except for those particular cases explicitly mentioned at due time. The main calculated electronic properties of neutral and charged $Co_nO_m^{0/+}$ clusters are collected in Tables 1-2. Some of these properties are represented in figures as functions of the number m of oxygen atoms in the cluster. Thus, the binding energy per atom of charged $Co_nO_m^+$ clusters is given in Figure 5, and the second total energy difference of neutral and charged $Co_nO_m^{0/+}$ clusters is given in Figure 6. These magnitudes are defined as:

$$E_b(n,m) = [n \times E(Co) + m \times E(O) - E(n,m)]/(n+m)$$

and

$$\Delta_2(n,m) = E(n,m-1) + E(n,m+1) - 2 \times E(n,m),$$

respectively, where $E(n,m)$ is the total energy of the (n,m) cluster. For a given n, the values $\Delta_2(n,m)$ as a function of m will show a prominent positive peak at those m values whose corresponding (n,m) clusters are more stable than their $(n,m-1)$ and $(n,m+1)$ neighbors against the addition or substraction of one oxygen atom.

As very general relations between geometry, calculated energy, and bonding distances in (n,m) clusters we enlighten the following ones, which are extracted from the discussion in the subsections below. 1) For $n \leq 5$, the oxygen atoms occupy face (bridge) sites of the Co subcluster when $m < n$ ($m \geq n$); for (4,7) clusters there are not enough bridge sites for all the oxygen atoms. 2) The binding energy of (3,m), (4,m), and (5,m) clusters increases as the average Co-Co distance increases. For (4,m), and (5,m) clusters the binding energy increases as the average Co-O distance decreases. For example, these rules are fulfilled along the series (5,m = 1-7), and comparing (5,8) with (5,7) we see that the binding energy decreases, the Co-Co distance decreases, and the Co-O distance increases. The case of (4,5) compared to (4,4) is an exception because the binding energy and the Co-O distance increase whereas the Co-Co distance decreases. From the trends above it can be said that the "covalent" bond between Co atoms contribute less than the "ionic" Co-O bond to the (n,m) cluster stability as both n and m increase.

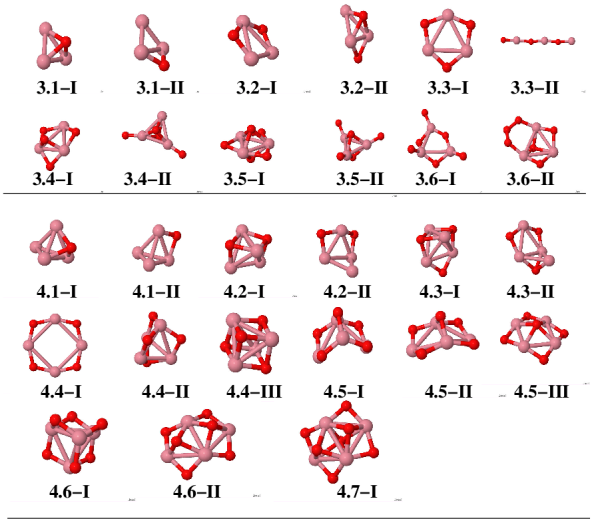

Fig. 1 (Color online) Low-energy isomers of $[Co_nO_m]^+$ with n=3,4 and m = 1-7. The notation is $n.m$-Label, with Label in roman letters in decreasing order of stability for each (n,m). Pink and red colors denote cobalt and oxygen atoms, respectively.

For $(n = 6-8, m)$ the relation between binding energy and Co-Co and Co-O bonding distances is not apparent. An interesting relation occurs for the 7.m-I clusters between the magnetic moment and the location of the oxygen atoms. Thus, the magnetic moments is 16 μ_B (m = 1-4), 18 μ_B (m = 5), and 12 μ_B (m = 6-10), and the locations of the oxygen atoms is, respectively, on faces (m = 1-5) and face or bridge sites (m = 6-10) of the subjacent Co_7 subcluster. The maximum magnetic moment, 18 μ_B at m = 5, can be related to the special geometry of two intertwined Co_5 and O_5 subclusters.

3.1.1 $[Co_3O_m]^+$, m = 1-6.

The (3,m) isomers in Figure 1 have a triangular core of Co atoms (except the linear 3.3-II isomer), with the oxygen atoms preferentially occupying bridge positions. The exceptions are: 3.1-I, with the oxygen on the hollow site of the triangle; 3.5-I, with two O on hollow (up and down sites); and 3.6-I with three oxygen in bridge sites and the other three on top positions. The O_3 substructure appearing in the 3.6-II isomer is an exception in all the stable isomers found in this work. The 3.2-I and 3.3-I isomers are planar. In 3.3-I and 3.5-I the triangle of Co atoms is equilateral.

The stoichiometric 3.3-I cluster shows higher symmetry (D_{3h}), binding energy per atom, magnetic moment, Kohn-

Table 1 Several properties of neutral and cationic $Co_nO_m^{0/+}$ clusters (n = 3-6; m = 1-9): Sym = molecular symmetry; $E_b(n,m)$ = binding energy per atom (eV); μ = magnetic moment in Bohr magnetons (μ_B); I_p = ionization potential (eV); H-L = Kohn-Sham gap (eV).

$n.m$-i		neutral/cation			
isomer	Sym	$E_b(n,m)$	μ	I_p	H-L gap
3.1-I	C_{3v}	3.00/3.42	7/6	6.54	0.15/0.50
3.1.II	C_s	3.08/3.33	7/8	7.25	0.41/0.26
3.2-I	C_{2v}	3.63/3.82	9/8	7.28	0.41/0.51
3.2-II	C_s	3.54/3.78	7/8	7.02	0.26/0.37
3.3-I	C_{2v}/D_{3h}	4.11/4.09	9/10	8.35	0.58/0.40
3.3-II	$C_{\infty v}$	3.67/3.74	9/10	7.79	0.26/0.00
3.4-I	C_s	4.04/3.97	7/8	8.72	0.52/0.33
3.4-II	C_{2v}	3.90/3.81	5/6	8.79	0.49/0.50
3.5-I	D_{3h}	3.98/3.86	7/8	9.17	0.45/0.17
3.5-II	C_s/C_1	3.98/3.81	5/6	9.58	0.47/0.51
3.6-I	C_s	4.05/3.97	7/4	9.35	0.45/0.15
3.6-II	C_s	3.93/3.87	7/8	8.78	0.51/0.30
4.1-I	C_s/C_{3v}	3.12/3.48	8/9	6.42	0.34/0.19
4.1-II	C_{2v}/C_s	3.11/3.40	8/9	6.79	0.19/0.19
4.2-I	C_{2v}/C_{3v}	3.60/3.82	10/9	6.90	0.24/0.46
4.2-II	C_s	3.63/3.72	10/11	7.67	0.50/0.04
4.3-I	C_s	3.93/4.07	8/11	7.23	0.40/0.27
4.3-II	C_s	3.93/4.04	10/11	7.49	0.33/0.47
4.4-I	D_{4h}	4.25/4.21	12/13	8.54	0.49/0.50
4.4-II	C_s	4.12/4.14	10/11	8.01	0.00/0.18
4.4-III	T_d	4.05/4.14	12/13	7.52	0.39/0.12
4.5-I	C_{2v}	4.19/4.22	6/7	7.98	0.28/0.56
4.5-II	C_{2v}	4.23/4.19	10/9	8.50	0.51/0.47
4.5-III	C_{4v}	4.18/4.15	6/7	8.48	0.34/0.38
4.6-I	C_s/C_{2v}	4.30/4.28	6/5	8.39	0.44/0.56
4.6-II	C_s/C_{2v}	4.13/4.10	10/11	8.48	0.34/0.52
4.7-I	C_{2v}/C_s	4.09/3.96	10/9	9.60	0.48/0.29
5.1-I	C_s	3.22/3.51	11/10	6.44	0.21/0.26
5.1-II	C_s	3.21/3.48	11/10	6.59	0.27/0.21
5.1-III	C_s	3.20/3.46	11/10	6.70	0.29/0.26
5.2-I	C_1	3.64/3.82	11/12	6.98	0.25/0.29
5.2-II	C_1	3.64/3.81	11/12	7.01	0.29/0.30
5.3-I	C_s	3.95/4.04	13/12	7.55	0.24/0.38
5.3-II	C_s/C_1	3.93/3.99	13/14	7.72	0.23/0.29
5.4-I	C_{2v}	4.22/4.24	13/14	8.13	0.36/0.43
5.4-II	C_s/C_1	4.04/4.07	11/10	7.94	0.35/0.23
5.5-I	C_s	4.25/4.30	11/12	8.35	0.28/0.78
5.5-II	C_1/C_{2v}	4.24/4.29	15/2	7.80	0.27/0.41
5.5-III	C_s	4.22/4.21	11/12	8.30	0.29/0.27
5.6-I	C_{2v}	4.34/4.31	11/10	8.54	0.25/0.41
5.6-II	C_1	4.30/4.27	9/10	8.55	0.36/0.11
5.6-III	C_s/C_1	4.24/4.25	15/16	8.16	0.28/0.27
5.7-I	C_1/C_s	4.35/4.35	9/10	8.20	0.31/0.38
5.7-II	C_1/C_s	4.33/4.31	7/8	8.41	0.37/0.13
5.8-I	C_{2v}/C_s	4.33/4.31	9/8	8.48	0.26/0.34
6.1-I	C_{3v}	3.39/3.59	14/13	6.87	0.35/0.17
6.1-II	C_{2v}	3.37/3.56	14/13	6.89	0.25/0.15
6.2-I	C_{2v}	3.74/3.90	14/13	6.94	0.18/0.00
6.3-I	C_{3v}	4.06/4.17	14/15	7.28	0.23/0.49
6.4-I	T_d	4.34/4.35	14/13	8.06	0.67/0.07
6.4-II	D_{2h}	4.11/4.21	14/15	7.22	0.18/0.06
6.5-I	C_s	4.27/4.31	16/15	7.83	0.15/0.23
6.5-II	C_s	4.27/4.30	16/17	7.87	0.21/0.24
6.5-III	C_{3v}	4.28/4.30	14/15	7.99	0.10/0.31
6.6-I	C_{2v}	4.31/4.38	14/19	7.40	0.31/0.17
6.6-II	C_{2v}	4.29/4.37	12/15	7.31	0.28/0.42
6.6-III	D_{3h}/C_{2h}	4.29/4.30	12/15	8.15	0.36/0.24
6.7-I	C_1/C_s	4.35/4.38	8/15	7.89	0.26/0.12
6.7-II	C_s/C_{3v}	4.36/4.34	10/11	8.49	0.25/0.21
6.8-I	O_h	4.44/4.38	10/11	8.89	0.24/0.46
6.8-II	D_{4h}	4.29/4.25	16/13	8.84	0.19/0.26
6.9-I	C_{4v}	4.36/4.45	10/11	6.91	0.39/0.33

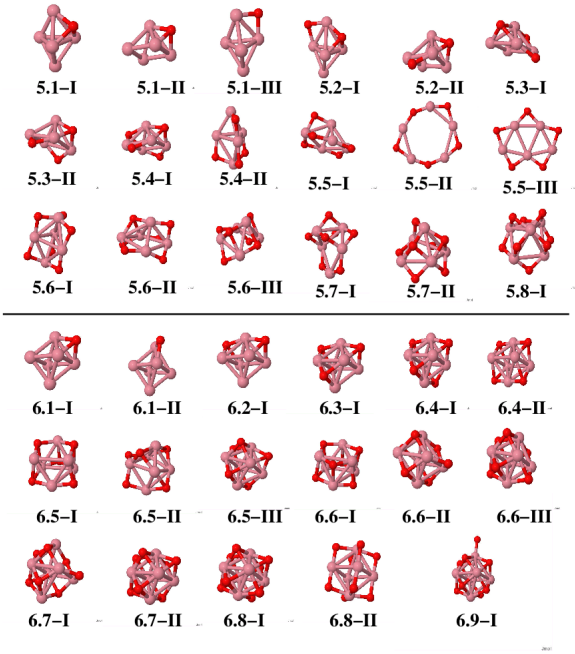

Fig. 2 (Color online) Low-energy isomers of $[Co_nO_m]^+$ with n=5,6 and m = 1-9. The notation as in Fig. 1.

Sham gap, and second energy difference than its neighbors, as can be seen in Table 1 and Figure 5. We will see in the subsections below, that the 3.3-I structure is a motif appearing in the structure of the larger (n $\leq$ 6,m) clusters. The average Co-Co inter-atomic distance in (3,m) clusters is larger than in the pure Co_3^+ (2.267 Å). That distance increases with m = 1, 2, and 3 (2.350 Å, 2.653 Å, and 2.780 Å), and then decreases for m = 4, 5 (2.656 Å and 2.456 Å). For m = 6, with 3 oxygen on top and 3 in bridge, the average Co-Co distance increases again (2.915 Å). On the other hand, the average Co-O distance oscillates along m = 1-6: 1.870, 1.790, 1.810, 1.804, 1.897, and 1.723 (in Å). The calculated distance for CoO^+ molecule is 1.67 Å, which is smaller (larger) than the Co-O distance in bridge (top) site of cobalt oxide clusters.

3.1.2 $[Co_4O_m]^+$, m = 1-7.

The 4.4-I cluster, with a very stable D_{4h} planar structure, is a singular exception in the (4,m) series of clusters, which are generally three-dimensional. The high stability of 4.4-I, as shown by the binding energy, ionization potential, Kohn-Sham gap, and second energy difference (see Table 1 and Figure 6), agrees with the special abundance of that cluster in the experimental fragmentation spectra.[16] The planar structure was confirmed by ion mobility mass spectrometry experiments.[10] The high magnetic moment of that ring structure will be thoroughly commented in section 3.3 below. Except 4.4-I, all the

(4,m) isomers in figure 1 are based on a three dimensional skeleton of Co atoms, which is near tetrahedral for m = 1-3, and m = 6, but it forms a near planar (butterfly like) Co_4 subcluster for the (4,5) and (4,7) isomers. The favorable site for oxygen atom is bridging two Co atoms (see for example in 4.4-I and 4.6-I in Figure 1).

The average Co-Co distance increases along m = 1-4 (2.43, 2.53, 2.59, and 3.01 (in Å)) and decreases for m = 4-6 (2.714, 2.63, and 2.583 (in Å)). Instead, the average Co-O distance decreases along m = 1-5 (1.910, 1.903, 1.895, 1,780, 1.764, (in Å)), and increases for m = 6-7 (1.765, 1.871 (in Å)). These trends point to a delicate compromise between the contribution of Co-Co and Co-O units to the cluster binding properties.

3.1.3 $[Co_5O_m]^+$, m = 1-8.

All the $Co_5O^+_{1-8}$ isomers in Figure 2 are three dimensional except 5.5-II and 5.5-III. Note that 5.5-II has only 10 meV smaller binding energy per atom than the ground state 5.5-I structure, but a magnetic moment of only 2 μ_B (compared to 12 μ_B for 5.5-I. The ground state 5.5-I has a basis formed by the planar 4.4-I and a CoO unit on that planar motif. In fact, we will comment later, in the section devoted to fragmentation properties, that the most favorable fragmentation of 5.5-I isomer is the loss of a CoO molecule, which agrees with the experiments.[16] On the other hand, the isomer 5.5-I shows the highest Kohn-Sham gap within this series (see Table 1), which is a signature of special stability against the change of its electronic charge. However, regarding the content of oxygen atoms, the second energy differences for (5,m) clusters at m = 5 in Figure 6 doesn't show any special feature with respect to its neighbors 5.4-I and 5.6-I. In the putative ground states of $Co_5O^+_{1-8}$, those clusters with m = 1,2, and 6 show hexahedral symmetry for the Co_5 subcluster, while for the other oxides it has square pyramid symmetry. It is interesting to inspect the preferred oxygen sites as increasing oxygen loading. For m = 1, the oxygen atom occupies a hollow site (coordinated to three Co atoms), and for m = 2 the second oxygen is in a bridge position opposite to that hollow site. For m = 3 (4), two O atoms sit on opposite triangular faces, and the third (four) O is in a bridge site. For m = 5-8 all the oxygens occupy bridge sites. The average Co-Co distances for m = 1-8 are (in Å) 2.398, 2.494, 2.474, 2.535, 2.6025, 2.623, 2.771, and 2.729, respectively, whereas the Co-O average distances are (in Å) 1.913, 1.868, 1.879, 1.870, 1.775, 1.770, 1.762, 1,770, respectively. Note that for 5.6-III we obtain the maximum spin magnetic moment of this series (16 μ_B).

3.1.4 $[Co_6O_m]^+$, m = 1-9.

The lowest energy configurations in this series have a Co_6 subcluster decorated with oxygen atoms. For m = 1-4 and 8-9 that subcluster is octahedral like, and the consecutive O atoms occupy hollow sites, except m = 9 because there is no more available hollow sites and the ninth oxygen binds then to atop

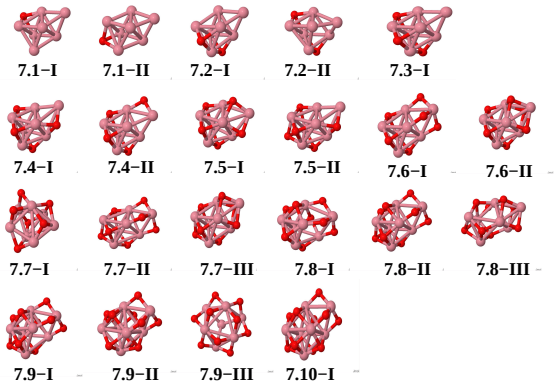

Fig. 3 (Color online) Low-energy isomers of $[Co_nO_m]^+$ with n=7 and m = 1-10. The notation as in Fig. 1.

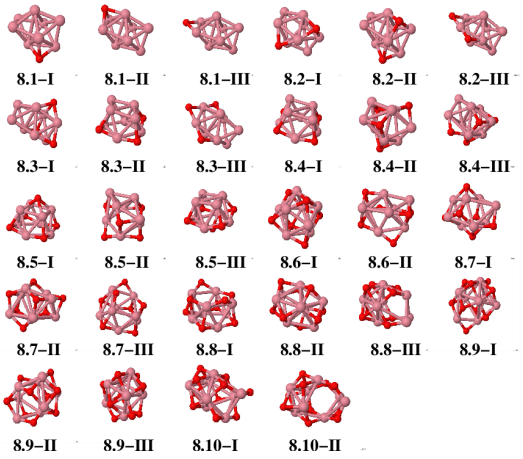

Fig. 4 (Color online) Low-energy isomers of $[Co_nO_m]^+$ with n=8 and m = 1-10. The notation as in Fig. 1.

Table 2 Several properties of neutral and cationic $Co_nO_m^{0/+}$ clusters (n = 7-8; m = 1-9); labels of columns as in Table 1.

$n.m$-i		neutral/cation			
isomer	Sym	$E_b(n,m)$	μ	I_p	H-L gap
7.1-I	C_s	3.44/3.65	15/16	6.53	0.23/0.27
7.1-II	C_{3v}	3.39/3.59	17/16	6.68	0.28/0.32
7.2-I	C_s	3.77/3.93	15/16	6.79	0.23/0.29
7.2-II	C_1	3.74/3.90	15/16	6.75	0.15/0.28
7.3-I	C_{3v}	4.08/4.17	15/16	7.29	0.37/0.32
7.4-I	C_s	4.20/4.31	15/16	7.09	0.18/0.34
7.4-II	C_s	4.19/4.28	15/16	7.32	0.16/0.41
7.5-I	C_s	4.29/4.38	15/18	7.12	0.22/0.21
7.5-II	C_s	4.17/4.25	15/16	7.34	0.24/0.27
7.6-I	C_{3v}	4.44/4.47	11/12	7.89	0.27/0.31
7.6-II	C_{3v}	4.35/4.41	15/18	7.50	0.24/0.13
7.7-I	C_s	4.38/4.43	15/12	7.53	0.18/0.20
7.7-II	C_s	4.38/4.42	11/12	7.73	0.12/0.29
7.7-III	C_{3v}	4.31/4.37	11/12	7.45	0.25/0.45
7.8-I	C_s	4.42/4.44	9/12	7.84	0.30/0.22
7.8-II	C_s	4.41/4.42	7/8	8.08	0.18/0.21
7.8-III	C_1	4.39/4.40	15/16	8.08	0.24/0.29
7.9-I	C_s	4.45/4.47	13/12	7.94	0.23/0.29
7.9-II	C_{3v}	4.43/4.43	7/10	8.19	0.32/0.12
7.9-III	C_{3v}	4.11/4.16	19/14	7.48	0.43/0.35
7.10-I	C_s	4.48/4.48	13/12	8.18	0.22/0.17
8.1-I	C_1	3.48/3.69	16/17	6.29	0.14/0.27
8.1-II	C_s	3.50/3.69	18/19	6.55	0.22/0.10
8.1-III	C_{2v}	3.48/3.65	18/19	6.77	0.27/0.03
8.2-I	C_1	3.72/3.90	16/17	6.41	0.15/0.22
8.2-II	C_s	3.73/3.90	18/17	6.47	0.09/0.13
8.2-III	C_s	3.75/3.86	18/19	7.07	0.22/0.16
8.3-I	C_s	4.00/4.13	16/17	6.84	0.16/0.20
8.3-II	C_s	3.96/4.07	18/19	6.94	0.23/0.20
8.3-III	C_{2v}	3.96/4.04	18/17	7.35	0.25/0.23
8.4-I	C_{2v}	4.17/4.26	18/19	7.19	0.15/0.16
8.4-II	C_s	4.09/4.21	16/17	6.84	0.18/0.21
8.4-III	C_2	4.09/4.18	16/17	7.16	0.15/0.30
8.5-I	C_{4v}	4.35/4.43	18/19	7.26	0.08/0.30
8.5-II	C_1	4.24/4.30	18/19	7.41	0.28/0.15
8.5-III	C_{2v}	4.18/4.27	20/21	7.10	0.19/0.25
8.6-I	C_{2v}/C_{4v}	4.35/4.43	20/17	7.18	0.03/0.30
8.6-II	C_2	4.37/4.34	20/17	8.69	0.23/0.21
8.7-I	C_s	4.38/4.44	20/21	7.32	0.13/0.18
8.7-II	C_1	4.37/4.43	18/19	7.35	0.27/0.22
8.7-III	C_1	4.38/4.42	20/21	7.63	0.18/0.20
8.8-I	C_{2v}	4.44/4.47	22/19	7.84	0.20/0.25
8.8-II	C_2/C_1	4.41/4.45	8/17	7.63	0.21/0.23
8.8-III	C_s	4.34/4.38	16/15	7.71	0.14/0.14
8.9-I	C_1	4.44/4.46	14/15	7.80	0.19/0.27
8.9-II	C_1	4.44/4.46	16/17	7.85	0.18/0.26
8.9-III	C_1	4.43/4.46	16/17	7.77	0.22/0.26
8.10-I	C_1	4.45/4.46	12/17	8.17	0.26/0.16
8.10-II	C_1	4.42/4.43	16/17	8.12	0.21/0.15

site. For m = 5-6, the Co_6 subcluster is a deformed octahedron, which we denote as tower-like, and for m = 7, that substructure is amorphous-like.

The average Co-Co distances are (in Å) 2.387, 2.428, 2.437, 2.402, 2.503, 2.773, 2.715, 2.420, and 2.636, for m = 1-9, respectively. The minimum (2.402 Å) appears for 6.4-I isomer with T_d symmetry, whose faces caped with an O atom have three first neighbor faces without O atom. That isomer shows a peak in the trend of binding energy per particle (Figure 5) and in the second energy difference (Figure 6). Note that the average Co-Co distance in the pure Co_6^+ octahedron is 2.390 Å. Thus, for $n \leq 6$ the cobalt oxide clusters have an inner core of highly coordinated Co leading to a binding energy higher than that of open near planar structures, which are dominated by Co-O bonds. Nevertheless, one can observe one or several quasi-planar Co_3O_3 substructures for m = 3-6 clusters. The average Co-O distance is (in Å) 1.917, 1.913, 1.913, 1.913, 1.930, 1.947, 1.906, 1.923, and 1.902, respectively, for m = 1-9. The smallest Co-O average distance for $m = 9$ is due to the atop oxygen on the octahedral Co_6 subcluster, which leads the largest binding energy per particle of this series.

The structure 6.8-I is a perfect octahedron (O_h) with the highest HOMO-LUMO gap in this series (together with the (C_{3v}) 6.3-I isomer). As for the 6.4-I isomer, the small Co-Co average distance (2.420 Å) is due to the geometrical shell closing effect. Note that the binding energy per atom of 6.6-I, 6.7-I, and 6.8-I is constant (4.38 eV) and that the magnetic moments are 19 μ_B, 15 μ_B, 11 μ_B respectively. These data indicates that the adding of one or two oxygen atoms to 6.6-I does not contribute to a larger binding energy per particle, but lowers the total magnetic moment.

3.1.5 $[Co_7O_m]^+$, m = 1-10.

We obtain minimum energy structures having a capped octahedron Co_7 subcluster for m = 1-7, and 10. For m = 8-9 that capped octahedron is deformed. The oxygen atoms bind on the triangular faces (coordinated to three Co atoms) for m = 1-7, and 10; others also occupy bridge sites. One or several Co_3O_3 and Co_4O_4 substructures can be identified in some of the clusters. The binding energy per particle of the 7.m-I clusters in Figure 3 and Table 2, shows a peak for 7.6-I. A higher HOMO-LUMO gap also appears for 7.6-I (with C_{3v} symmetry). The average Co-Co distance is (in Å) 2.409, 2.420, 2.419, 2.495, 2.559, 2.608, 2.639, 2.682, 2.729, and 2.715, for m = 1-10, respectively. Note that those distances increase as m increases, and are larger than the Co-Co average distance of a pure Co_7^+ with capped octahedron structure (2.391 Å) or decahedral structure (2.398 Å). On the other hand, the average Co-O distance is (in Å) 1.920, 1.915, 1.921, 1.909, 1.919, 1.837, 1.865, 1.863, 1.862, and 1.874, respectively, for m = 1-10. Those distances show an almost constant behavior around 1.91 Å from m = 1-5, and then decrease to a minimum for

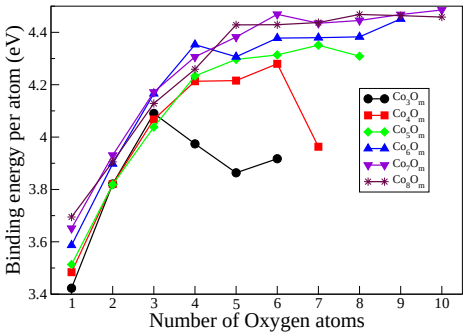

Fig. 5 (Color online) Binding energy per atom of cationic $Co_nO_m^+$ clusters as a function of the number of oxygen atoms.

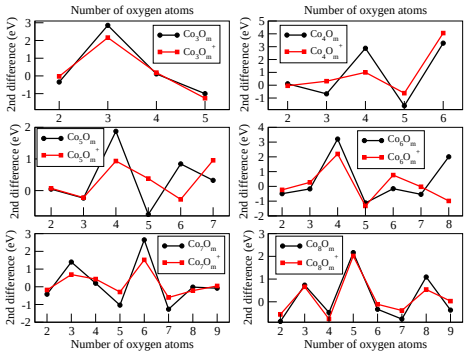

Fig. 6 (Color online) Second energy difference of neutral (black continuous line) and charged (red dashed line) $Co_nO_m^{0/+}$ clusters as a function of the number of oxygen atoms.

$m = 6$ followed by another regular behavior around 1.86 Å. For $m = 6$ it is observed a peak in the binding energy per particle (Figure 5) followed by a nearly flat behavior. Thus, the addition of more oxygen atoms to 7.6-I does not contributes significantly to the stability of the 7.6-I species. This feature is also observed in the trend of the second energy differences (Figure 6).

3.1.6 $[Co_8O_m]^+$, m = 1-10.

As shown in Figure 4 the two dominant arrangements of atoms are i) the tower-like type (m = 4-6,8), and ii) the one based on a free dodecahedral Co_8 subcluster (m = 1,3,7). A deformed Co_8 subcluster is identified for m= 2 and 7. The case m = 10 shows an amorphous like arrangement of Co and O atoms. The oxygen atoms prefer to bind on faces, except a few cases where two (m =8-9) or three (m = 10) oxygens bind in bridge positions. The largest binding energy per atom in this series corresponds to the stoichiometric 8.8-I (C_{2v}) isomer. It has also the largest magnetic moment (19 μ_B) in the series 8.m-I. This confirms the tendency to stabilize the ground state isomer with a large magnetic moment. The isomer 8.5-I has the largest HOMO-LUMO gap and also the largest peak in the second energy difference (Figure 6). The distribution of Co-Co and Co-O distances reflects somehow the form of the Co subcluster structure and the O bonding site. For m = 1-10, the Co-Co distance is (in Å), 2.437, 2.579, 2.450, 2.669, 2.441, 2.417, 2.617, 2.577, 2.710, and 2.673, respectively. On the other hand, for m = 1-10 the average Co-O distance is (in Å) 1.917, 1.903, 1.918, 1.896, 1.936, 1.968, 1.823, 1.875, 1.876, and 1.877, respectively. The relative minima (maxima) in the Co-Co (Co-O) distances correlate with the peaks in the second energy difference shown in Figure 6. This fact can be related to the stronger effect of Co-Co bonds compared to Co-O bonds to produce the compact type of geometries discussed above.

3.2 Fragmentation patterns

In Figure 7 are represented, as functions of the number of cobalt atoms, the threshold energies needed to separate the $Co_nO_m^+$ clusters into two fragments according to different channels: i) Co + $Co_{n-1}O_m^+$; ii) CoO + $Co_{n-1}O_{m-1}^+$; iii) CoO_2 + $Co_{n-1}O_{m-2}^+$; iv) O + $Co_nO_{m-1}^+$; and v) O_2 + $Co_nO_{m-2}^+$. These energies are defined as

$$E(Co_nO_m^+) - E(Co) - E(Co_{n-1}O_m^+)$$

for channel i), and similarly for the other fragmentation channels. In this work we don't calculate fission barriers. Thus, the threshold energy is the minimum energy needed for the fragmentation of a specific cluster according to a given channel. In the panels a), b), c), and d) of Figure 7 are represented those fragmentation energies for $Co_nO_m^+$ in the range n = 4-8 with $m = n-1, m = n, m = n+1$, and $m = n+2$, respectively. The separation of a cobalt or an oxygen atom are the less favorable channels, except for the $Co_5O_4^+$ cluster whose preferable channel is the detachment of a Co atom.

In Figure 8 is compared the most favorable fragmentation channel from our calculations with the one extracted from the strong fragmentation signals in the branching ratios of the photodissociation mass spectra (see Table 1 of Duncan and coworkers [16]). Both of them, calculation and experiment, show that the most favorable fragmentation channel is the separation of a molecular O_2 unit, with few exceptions which are attributable to the favorable formation of clusters with (n,n) stoichiometry. [14,16] These exceptions are the favored channels: i) (4,3) → (3,3) + Co, and (4,4) → (3,3) + CoO, which are both in agreement with the experimental results of Freas *et al* [14]; ii) (5,4) → (4,4) + Co and (5,5) → (4,4) + CoO, which are both in agreement with the experimental results of Duncan *et al.* [16] Note that fragmentation energy of the (5,4) → (4,3)

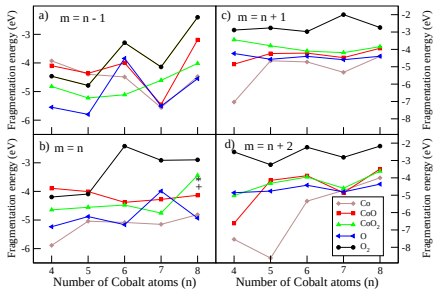

Fig. 7 (Color online) Threshold energies for the fragmentation of $Co_nO_m^+$ clusters (with n = 4-8 and $m = n-1$ (panel a), $m = n$ (panel b), $m = n+1$ (panel c), and $m = n+2$ (panel d)), for the separation of Co, CoO, CoO_2, O, and O_2 neutral fragments. The asterisk (*) and the cross (+) in panel b) correspond to the (8,8) $\rightarrow$ (4,4) + Co_4O_4 and (8,8) $\rightarrow$ (5,5) + Co_3O_3 channels, respectively (* = 3.76 eV; + = 3.94 eV).

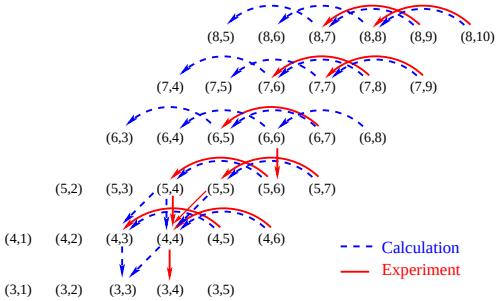

Fig. 8 (Color online) $Co_nO_m^+$ clusters, denoted here as (n,m), with increasing n (m) in the vertical (horizontal) direction, are connected by lines from parent to daughter according to the most favorable fragmentation channel: experimental results [16] (continuous -red- lines) versus calculation (dashed -blue- lines) are compared.

+ CoO channel is nearly equal to that of (5,4) $\rightarrow$ (4,4) + Co (see Figure 7a). However, only the channel rendering the (4,4) fragment is detected with a strong intensity signal.

On the other hand, the observed most prominent fragmentation channel [16] for those (n,n) clusters with n = 4, 6, and 8, are (4,4) $\rightarrow$ (3,4) + Co, (6,6) $\rightarrow$ (5,6) + Co, and (8,8) $\rightarrow$ (4,4) + Co_4O_4, respectively. Instead, for (4,4) we obtain (4,4) $\rightarrow$ (3,3) + CoO as the prominent channel, in agreement with the experiments of Freas *et al.* [14] Note that for the (4,4) $\rightarrow$ (3,2) + CoO_2 channel, which signal is also observed by Duncan *et al* [16], we obtained the third lower fragmentation energy (see Figure 7b). Similarly, the observed fragmentation channels of (6,6) rendering (5,6), (5,5), (5,4), and (4,4) fragments [16] are predicted in our calculations as those with the forth, second, third, and first lower threshold energies, respectively. The fragmentation of the (8,8) cluster deserves a few comments. First, notice in Figure 7-b that the four fragmentation channels with low threshold energy are those leading to the fragments (8,6), (7,6), (4,4), and (5,5), which are all them detected in the experiments (see Table 1 in the work of Duncan and coworkers [16]). We see that the second and third threshold energies (at 0 K), corresponding to the release of CoO_2 and Co_4O_4 neutral fragments, respectively, are nearly degenerate. On the other hand, in addition to the threshold energy an important factor will be the transition barrier which can be different for the various fragmentation channels. Thus, the transition from the three-dimensional geometry of the (8,8) parent towards two planar fragments, that is, $Co_4O_4^+$ + Co_4O_4, may be hindered by a high transition barrier (from symmetry considerations), but the transition barrier towards the three dimensional 4.4-II or 4.4-III isomers can be smaller.

Among the not specially prominent but observed channels (Table 1 in Duncan *et al*, [16]) we have predicted most of them as low lying threshold energy channels (and then favorable, in principle). In the following we comment briefly on these fragmentation channels, within a simplified notation: (4,5) $\rightarrow$ (4,4) is our third channel; (4,5) $\rightarrow$ (3,3) is the second one; (4,6) $\rightarrow$ (3,4) is the third; (5,5) $\rightarrow$ (4,3) is the third; (5,5) $\rightarrow$ (3,3) + Co_2O_2 has an threshold of -3.926 eV, which is only 20 meV smaller than that for the preferred channel (5,5) $\rightarrow$ (4,4); (5,6) $\rightarrow$ (4,4) is the second channel; (5,7) $\rightarrow$ (5,5), which is the only observed channel for (5,7) cluster, has an threshold -3.242 eV, very close to the threshold for the loss of O_2; (6,6) $\rightarrow$ (5,5) is the second preferred channel; (6,6) $\rightarrow$ (4,4) and (6,6) $\rightarrow$ (5,4) are the third and fourth channels respectively; in addition to the most prominent (6,5) cluster observed from (6,7) fragmentation, there are observed the fragments (5,5), (5,6), (6,6), (5,7) (whose threshold energies are in the range -4.096 eV to -4.722 eV); (6,8) $\rightarrow$ (5,6) and (6,8) $\rightarrow$ (6,7) are predicted with -3.950 eV and -4.424 eV, respectively; from (7,7) are observed the fragments (6,7), (6,6), and (6,5) whose threshold energies are $\sim$ 4.3-5.1 eV; from (7,8) and (7,9) the loss of O_2 is the observed prominent fragmentation, as predicted in our calculations; the others observed fragmentations from (7,8) and (7,9) are predicted with threshold energies $\sim$ 4.2-5.4 eV; for (8,8) we have already commented the main aspects of the observed versus calculated fragmentation channels, respectively; for (8,9) are observed fragmentation channels leading to (8,7), (7,7) and (7,9) clusters, which are our first, second, and fourth more favorable channels; the observed fragmentation channels of (8,10) lead to (8,8), (7,9) and (7,8) clusters, corresponding to our first, second, and fourth more favorable channels. In summary, we have obtained an overall good qualitative explanation of a big collection of observed data [14,16] for the fragmentation of cobalt oxide clusters.

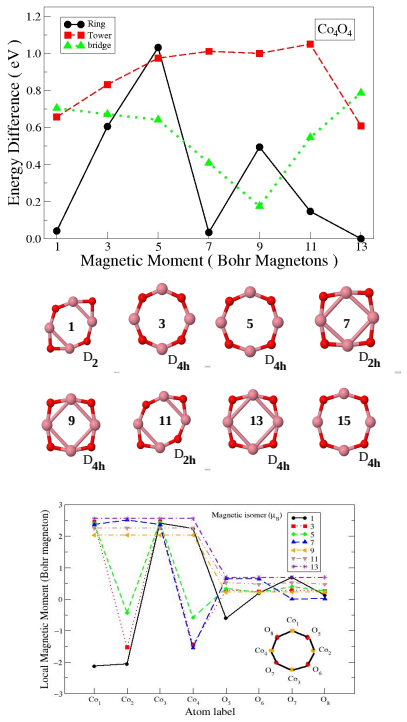

Fig. 9 (Color online) In the upper panel is given the energy relative to that of the ring-like ground state for the magnetic isomers of $Co_4O_4^+$ having planar (dots), tower-like (squares), and bridge-like (triangles) structural arrangements. In the middle panel are depicted the spin isomer geometry of the ring-like (planar) family. In the lower panel is given the local magnetic moment for the isomers of that ring-like family.

3.3 Magnetic properties

In Tables 1-2 is given the spin magnetic moment of each cluster. As a general trend, the maximum total magnetic moment increases as increasing the number of Co atoms due to the ferromagnetic-like coupling of the ground state of most clusters. Low spin magnetic moments are obtained for certain oxygen compositions, as a consequence of antiparallel magnetic couplings within the cluster. The spin isomeric map of cobalt oxide clusters is complex with oscillations in many cases. An illustrative example of these facts is $(CoO)_4^+$ that we analyze below. We note that the change of magnetic moment as going from the neutral cluster to its positively charged counterpart amounts in general to $1\mu_B$.

Our results confirm the experimental observation of abundance of certain clusters as the final product of fragmentation channels of different cobalt oxide clusters. The most notorious example is the stoichiometric cluster $(CoO)_4^+$. A detailed analysis of this cluster is, therefore, pertinent in order to understand its high stability in relation with its structural and electronic properties. We have considered three structural families (monocyclic-ring, tower-like and cubic-like) as input for this cluster, and several possible spin magnetic states (total magnetic moments from 1 to 13 μ_B). A full structural relaxation was performed for each spin state. The upper panel of Fig. 9 shows the energy difference of each structural and/or spin isomer with respect to the putative ground state that is the monocyclic-ring structure with total magnetic moment of $13\mu_B$. The local magnetic moments distribution reported in the lower panel of Fig 9 indicates that in the ground state the magnetic couplings are parallel, each Co atom contributes with $2.56\mu_B$ and each O with $0.69\mu_B$. We note that oxidation does not quench the spin-polarization of the Co atoms since the per atom spin moment of the pure Co_4 cluster is $2.5\mu_B$ [24,25], and that of the cationic Co_4^+ is $2.50\mu_B$. Since in the ground state monocyclic-ring structure the magnetic couplings are parallel, the oxygen atoms also contribute to the total moment of $13\mu_B$ which results to be $4\mu_B$ higher that in the pure Co_4^+. All together leads $(CoO)_4^+$ to be a quite stable and symmetric bidimensional magnet, an interesting result indeed.

Low-energy isomers (up to 50meV) correspond to spin excitations (spin isomers of the monocyclic-ring structure). Those excitations lower the total spin state down to 7 and $1\mu_B$ as a consequence of the appearance of antiparallel magnetic couplings (Fig. 9) and can be qualified therefore as spin flip excitations. These are present in more or less degree for all the spin isomers with total moments lower than $9\mu_B$ (spin isomers with total moments higher than $7\mu_B$ are ferromagnetic-like). The stabilization of antiparallel magnetic couplings with certain magnetic arrangements is concomitant with structural relaxations that brake the symmetry of the ferromagnetic-like ground state in a way that allows to accommodate the antiparallel Co-Co couplings in such arrangements and to reduce the magnetic frustration in a large extent (note that Co is a ferromagnet). These effects can be clearly appreciated in Fig 9. In the $7\mu_B$ spin state, the magnetic moment of one Co atom points in opposite direction to the rest, so that this Co atom is further away from the rest as enlarging the Co-Co interatomic distance is a way of reducing the magnetic coupling. In the $1\mu_B$ spin state, two separated Co dimers are formed, with parallel magnetic coupling within each dimer and antiparallel inter-dimer coupling. The separation of the two Co dimers allows for reducing their mutual magnetic coupling. In order to quantify the energy cost of such Co-Co antiparallel magnetic couplings that the structural relaxation relieve, we have conducted two crosscheck structure- and total spin-fix calculations. We imposed a total magnetic moment of $1\mu_B$ with the geometrical structure of the ground state, and the reverse, a spin moment of $13\mu_B$ with the distorted geometrical structure of the $1\mu_B$ spin isomer. The electronic selfconsistent calculations led to spin-dependent charge densities consistent

with the imposed constrains but with a total energy difference of about 0.7eV with respect to the ground state, in both cases. This crosscheck highlights the strong stability of the monocyclic-ring structure, since the resulting arrangements, despite not being fully relaxed due to the imposed constrains, have stabilities comparable to those of the fully relaxed tower-like and cubic-like isomers in the same respective spin states which lie at about 0.6-0.8eV from the ground state (see Figure 9). In the $3\mu_B$ spin state of this structure, the antiparallel couplings are alternated so that a symmetric ring but with all Co-Co inter-atomic distances enlarged (distances comparable to the inter-dimer distance in the $1\mu_B$ spin state) is obtained. Short Co-Co distances are not compatible with antiparallel magnetic coupling between those Co atoms.

The first structural isomer appears at 0.18eV above the ground state and has cubic-like structure (isomer 4.4-II in Fig. 2) and total moment of $9\mu_B$. It is not expected to coexist with the ground state at room temperature. Tower-like clusters (isomer 4.4-III in Fig. 2) are quite unstable in all spin states for this cluster size. These two three-dimensional structural families present a lower degree of relaxation as changing the spin state (with antiparallel couplings also in the low spin states) than the bidimensional monocyclic-ring one, as it can be inferred from the comparison of inter-atomic distances. Our results indicate that the oxidation favors low-dimensional structures since the pure Co_4^+ cluster is three-dimensional and more compact. Since in the ground state monocyclic-ring structure the magnetic couplings are parallel, the oxygen atoms also contribute to the total moment. This together with the fact that Co moments are not quenched, lead $(CoO)_4^+$ to be a quite stable and symmetric bidimensional magnet.

We have conducted similar calculations for all stoichiometric $(CoO)_n^+$ clusters with $(n = 2-6)$ for the two families of isomers. In Fig. 10 we report the energy difference of each structural and/or spin isomer with respect to the putative ground state, and Fig. 11 shows all data for $(CoO)_2^+$, the smallest cluster with monocyclic-ring structure. We see no need to enter the same detail as in $(CoO)_4^+$. The map of spin isomers is rather complex in general, with oscillations in the energy as a function of the total magnetic moment in several cases. The bi-dimensional (2D) monocyclic-ring structure becomes less stable than the three-dimensional (3D) cubic-like for $n \geq 5$. The resulting total spin-moment as a function of cluster size is not monotonous and we find in most cluster-sizes low-energy spin flip excitations that allow configurations with low total spin magnetic moment very close in energy to the ground state. This 2D to 3D transition as a function of cluster size is consistent with ion mobility mass spectrometry measurements of Ota and coworkers.[10] These authors provide also DFT results for the cationic clusters (Gaussian with 6-31+G(d) basis set and B3LYP functional), although only for a few low-spin spin states and without details of the local magnetic moments

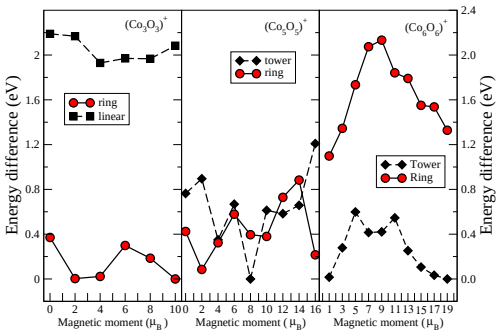

Fig. 10 (Color online) In the left panel is given the energy relative to that of the ground state for the magnetic isomers of $Co_3O_3^+$ having ring (dots) and linear (squares) structures. In the middle panel is given the energy relative to that of the ground state for the magnetic isomers of $Co_5O_5^+$ having ring (dots) and tower-like (squares) structures. In the right panel is given the energy relative to that of the ground state for the magnetic isomers of $Co_6O_6^+$ having ring (dots) and tower-like (squares) structures. Note the roll of the magnetism in the transition from planar to three dimensional geometry.

distribution. They estimate the orientation averaged collision cross sections of both the monocyclic ring structures and the more compact ones finding a good agreement with the experiments. This gives compelling evidence of the high stability of the monocyclic ring arrangements at least for the smaller clusters like $(CoO)_4^+$. Our results do not agree with theirs in the spin state, probably due to their not having explored high-spin states. We do not agree either in the energy difference between certain isomers, which in their calculation amounts to one order or magnitude more than ours, and comparablewith the energy required for structural transitions. Even between low spin isomers of the same structural family for certain sizes, unusually huge energy differences of up to several eV are given by Ota and coworkers. For instance, their energy difference between the monocyclic rings of $(CoO)_5^+$ with spin multiplicities 1 and 3 (magnetic moments 0 and $2\mu_B$) is $8.23eV$ while ours is a bit less than $0.4eV$.

4 Conclusions

In this work we performed systematic DFT-GGA calculations of the geometrical, electronic, and magnetic properties of neutral and cationic $Co_nO_m^{0/+}$ clusters with n = 3-8 and m = 1-10. The ionic structures were determined after optimizing several initial geometries selected from previous pure Co clusters calculations, with consecutive adsorbed oxygen atoms, as well as geometries constructed by assembling several CoO units and adding subsequent oxygen atoms. Both neutral and charged oxide clusters tend to stabilize preferably with the $n = m$ stoi-

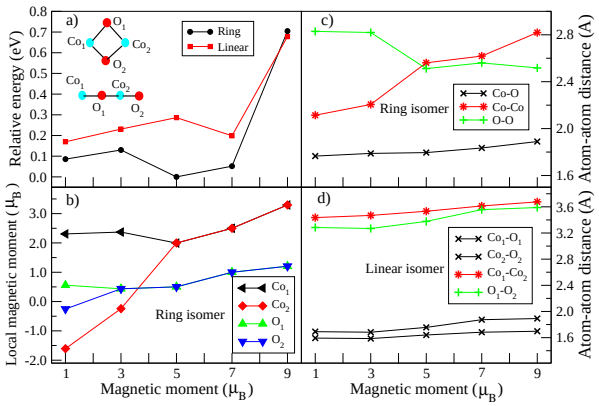

Fig. 11 (Color online) a) energy relative to that of the ground state for the magnetic isomers of $Co_2O_2^+$ having ring (dots) and linear (squares) structures; b) the local magnetic moment for the spin isomers of the ring-like family; in panels c) and d) are given the Co-Co, O-O, and Co-O bond distances for the spin isomers with ring and linear geometry, respectively.

chiometry, as shown by the computed binding energy per atom and by the trend of the second energy difference as a function of the oxygen content for a fixed number of cobalt atoms. That 1:1 stoichiometric relation is in agreement with the result from a recent multiphoton dissociation experiment of oxide clusters beams.[16]

The fragmentation patterns of these cobalt oxide cations were studied by comparing the energy separation of O_2, CoO, Co_2O, CoO_2, and Co fragments. We obtained that the preferred fragmentation channel is the loss of O_2, that the favorable stoichiometry is again 1:1, and that $Co_4O_4^+$ is especially stable, in full agreement with the experiments.[16] We have also predicted additional fragmentation channels, which can be a motivation for further experiments on this problem.

We also found that $(CoO)_n^+$ clusters are planar with monocyclic-ring structure for $n < 5$ and three-dimensional for larger sizes. This 2D to 3D transition as a function of size is in agreement with recent ion mobility experiments.[10] The trend with n of the calculated Co-Co and Co-O bond lengths is consistent with a transition from Co-O to Co-Co bond dominance in the stability of (m,n) clusters at $n \geq 6$. Such transition is directly linked to that from the planar geometry (based on CoO units) to the three dimensional geometry (based on a Co_n subcluster).

In addition, we obtained that the stoichiometric 1:1 $(CoO)_n^+$ clusters are further stabilized by a high magnetic moment. A detailed study of the spin isomers of these clusters, in particular the highly stable $(CoO)_4^+$ one, showed that: (i) oxidation does not quench the spin-polarization of the Co atoms and favors the planar structure, (ii) the isomeric map is complex, with oscillations corresponding to the existence of low-spin excited states, in some cases nearly degenerated with the high-spin state of the ground state, (iii) those low-spin states correspond to antiparallel magnetic couplings (spin-flip excitations) that are concomitant, in many cases, with structural relaxations that reduce the magnetic frustration, since short Co-Co distances are not compatible with antiparallel couplings, (iv) the change of magnetic moment as going from the neutral cluster to its positively charged counterpart amounts in general to $1\mu_B$.

We acknowledge the support of the Spanish "Ministerio de Ciencia e Innovación" and the European Regional Development Fund (Grant No. FIS2011-22957). F.A-G acknowledges financial support from PROMEP-SEP-CA230. R.H.A-T acknowledges the financial support provided by the University of Valladolid for a research visit and a fellowship from CONACyT (Mexico).

References

1 *Metal Oxides. Chemistry and Applications*, ed. L. G. Fierro, CRL, Boca Raton, FL, 2006.
2 A. Khodakov, B. Olthof, A. T. Bell and E. Iglesia, *Science*, 1996, **271**, 920.
3 C. Mordi, M. Eleruja, B. Taleatu, G. Egharevba, A. Adedeji, O. Akinwunmi, B. Olofinjan, C. Jeynes and E. Ajayi, *Journal of Materials Science and Technology*, 2009, **25**, 85.
4 A. Kirilyuk, K. Demyk, G. von Helden, G. Meyer, A. I. Poteryaer and A. I. Lichtenstein, *Journal of Applied Physics*, 2003, **93**, 7379.
5 A. Kirilyuk, A. Fielicke, K. Demyk, G. von Helden, G. Meijer and T. Rasing, *Phys. Rev. B*, 2010, **82**, 020405R.
6 C. van Dijk, *PhD. Thesis*, 2011, **Nijmegen**, The Netherlands.
7 D. J. Harding and A. Fielicke, *Chemistry*, 2014, **20**, 3258.
8 H.-J. Z. S. Li, L.-S. Wang, and D. A. Dixon, *J. Phys. Chem. A*, 2012, **116**, 5256.
9 H.-Q. Wang and H.-F. Li, *J. Chem. Phys*, 2010, **137**, 164304.
10 K. Ota, K. Koyasu, K. Ohshimo and F. Misaizu, *Chem. Phys. Lett.*, 2013, **588**, 63.
11 K. Ohshimo, T. Komukai, R. Moriyama and F. Misaizu, *J. Phys. Chem. A*, 2014, **118**, 3899.
12 E. L. Uzonova and H. Mikosch, *J. Phys. Chem. A*, 2012, **116**, 3295.
13 W. Jin, C. Li, G. Lefkidis and W. Hübner, *Phys. Rev. B*, 2014, **89**, 024419.
14 R. Freas, B. Dunlap, B. Waite and J. Campana, *J. Chem. Phys.*, 1987, **86**, 1276.
15 S-Yin, W. Xue, X.-L. Ding, W.-G. Wang, S.-G. He and M.-F. Ge, *Chem. Phys. Lett.*, 2009, **281**, 72.
16 C. J. Dible, S. T. Akin, S. Ard, C. P. Fowler and M. A. Duncan, *J. Phys. Chem. A*, 2012, **116**, 2691.
17 J. M. Soler, E. Artacho, J. D. Gale, A. G. a, J. Junquera, P. Ordejón and D. Sańchez-Portal, *J. Phys.: Condens. Matter*, 2002, **14**, 2745.
18 J. P. Perdew, K. Burke and M. Ernzerhof, *Phys. Rev. Lett.*, 1996, **77**, 3865.
19 N. Troullier and J. L. Martins, *Phys. Rev. B.*, 1991, **43**, 1993.
20 L. Kleinman and D. M. Bylander, *Phys. Rev. Lett.*, 1982, **48**, 1425.
21 S. G. Louie, S. Froyen and M. L. Cohen, *Phys. Rev. B*, 1982, **26**, 1738.
22 G. Kresse and J. Hafner, *Phys. Rev. B*, 1993, **47**, R558.
23 G. Kresse and J. Furthmüller, *Phys. Rev. B*, 1996, **54**, 11169.
24 S. Datta, M. Kabir, S. Ganguly, T. Saha-Dasgupta and A. Mookerjee, *Phys. Rev. B*, 2007, **76**, 014429.
25 J. L. Rodriguez-López, F. Aguilera-Granja, K. Michelian and A. Vega, *Phys. Rev. B*, 2003, **67**, 174413.